Preoperative Planning Algorithm for Robot-Assisted Minimally Invasive Cholecystectomy Combined With Appendectomy

TAO SONG [ID]1, **BO PAN** [ID]1, **GUOJUN NIU** [ID]2, **AND YILI FU**1, (Member, IEEE)

[1]State Key Laboratory of Robotics and System, Harbin Institute of Technology, Harbin 150001, China
[2]School of Mechanical Engineering and Automation, Zhejiang Sci-Tech University, Hangzhou 310018, China

Corresponding author: Bo Pan (mepanbo@hit.edu.cn)

ABSTRACT Preoperative planning for robot-assisted minimally invasive surgery is critical stage. Recently, many studies focus on the preoperative planning of the robot-assisted minimally invasive single-site surgery. However, the preoperative planning for the robot-assisted minimally invasive combined surgery based on the optimization algorithm has not been reported. In order to improve the dexterity and coordination of the manipulators in the surgical areas and to reduce the preoperative adjustment time for the combined surgery, this paper proposes a preoperative planning algorithm based on the non-dominated sorting genetic algorithm II (NSGA-II) for robot-assisted minimally invasive Cholecystectomy combined with Appendectomy (RAMICA). The preoperative planning algorithm simultaneously optimizes the entry ports and configurations of the manipulators. The optimization objective functions of the preoperative planning algorithm consist of a novel global dexterity index (GDI) based on the coefficient of variation and the coordination index (CI) that reflects hand-eye coordination and instrument coordination. The constraints of the preoperative planning algorithm include the port placement constraint and the non-collision constraint. The preoperative planning scheme based on the optimization algorithm are verified by comparative simulations to provide the better dexterity and coordination of the manipulators. Finally, the contrast experiments are carried out to demonstrate the effectiveness and superiority of the preoperative planning scheme obtained by the optimization algorithm.

INDEX TERMS Preoperative planning, robot-assisted minimally invasive surgery, Cholecystectomy combined with Appendectomy, NSGA-II optimization algorithm.

I. INTRODUCTION

Robot-assisted minimally invasive surgery (RAMIS) has been applied in a variety of surgical operations, due to its advantages such as high accuracy, less trauma, and less recovery time [1]. In addition, RAMIS can perform surgical operations with high coordination and dexterity, and thus improve surgical quality and safety [2]. Before the RAMIS, the locations of the entry ports and the configurations of the robot manipulators are the most critical issues in preoperative planning, which straightforwardly affect the dexterity and coordination of the instruments in the surgical areas and affect

The associate editor coordinating the review of this manuscript and approving it for publication was Hamid Mohammad-Sedighi [ID].

extracorporeal collisions. Improper entry ports and robot arm configuration may lead to add the new entry port, or more seriously may be converted to traditional open surgery. The optimal preoperative planning scheme can provide the better view and the better robot kinematic performances in the surgical areas. Therefore, preoperative planning is an important and significant stage to successfully perform the operation.

For decades, there are many research groups focus on the preoperative planning for RAMIS with respect to actual physiological structural features, instrument dexterity, and robot arm collision. A research direction for preoperative planning is based on the surgeon's clinical experiences. The Researchers gave some preoperative planning guidelines

according to the medical perspective, extensive clinical trials, and unexpected problems occurred during the surgery. Ferzli and Fingerhut [3] proposed a common method to place trocars properly. The anterior and lateral abdominal wall was divided into four quadrants corresponding to the classical divisions, plus two triangles [4]. The paper gave a detailed description of the surgical requirements and port placements according to different organs and surgical positions of every sub-area, and provided the reader with recommendations for safe, adapted, worker-friendly laparoscopic access to the abdominal cavity through a standardized methodology of trocar placement. Pick *et al.* [5] proposed the determination method of the entry ports of Da Vinci minimally invasive surgical robot system for Prostatectomy. Badani *et al.* [6] proposed the determination method of the entry ports of Da Vinci system for Nephrectomy. All the above preoperative planning methods are based on the surgeon's experiences, the robot performances and collision of manipulators in the surgical areas are less considered.

In order to automatically determine the locations of entry ports and the configurations of manipulators, another research direction is to improve the robot performances in the surgical areas. Cannon *et al.* [7] proposed a computer-based algorithm to optimize the port placements and robot placement according to tool dexterity and endoscopic view quality. The positions of the instrument ports and laparoscope port were determined by optimizing the weighted squared deviation of the instrument and endoscope angles. Adhami *et al.* [8] proposed an approach that consisted of planning, validation, and simulation. The validation step formed a solid guaranty of the results proposed in the planning. Finally, the simulation interface offered an intuitive tool to rehearse the intervention and comfort of the surgeon. In addition, Adhami and Coste-Manière, [9] put forward a two-step strategy to optimize the port placements and the pose of the robot. Two angles were mentioned in the optimization algorithm, the one angle was between the direction of an admissible location and the line relating a target to that admissible location, the other angle was between the direction of a target cone and the line relating that target to an admissible location. The dexterity and operability of the instrument were considered within the surgical area. Trejos and Patel [10] proposed an algorithm based on the global conditioning index and global isotropy index for determining the best port location and surgical robot configuration for endoscopic cardiac surgery. Azimian *et al.* [11] proposed multi-objective optimality criteria for Coronary Artery Bypass Grafting. The optimality criteria consisted of a clearance measure and a new collective kinematic measure. Two modified manipulability indices that were dimensionally homogeneous form the kinematic measure. The coordination was not discussed.

Li *et al.* [12] proposed a pose planning method that optimized the cooperative working space inside the abdomen to adjust the joint angles of the stationary joints. A maximum distance criterion was adopted to guarantee a collision-avoidance operation. The constraint that the fixed positions of entry ports were on the patient's abdominal wall was satisfied. However, the port placement was not discussed. Yu *et al.* [13] proposed a preoperative positioning method of the instrument arms' passive joints. Under the premise of the entry points being fixed positions, the forward and inverse kinematics were calculated to obtain the set of effective positioning results, and then the percentage of collaboration workspace of the two instrument arms was used to judge the best preoperative positioning angles. Feng et al [14] proposed an optimization method to optimize the port placements and robot pose. This method divided the port areas into many sub-areas. In each of the sub-area, the robotic arm configuration was solved using the optimization method and the operational workspace was calculated to obtain the best port placement and robot pose.

As discussed in the literatures, the aforementioned methods optimized the port placements and configurations of the manipulators by adopting the dexterity, the isotropy, the coordination of manipulators, cooperative workspace, and non-collision as optimization indexes. However, the above methods aimed at the single-site surgery. In fact, the combined surgery has many advantages [15], [16]. Firstly, the combined surgery performed by a group of entry ports can reduce the trauma and the incision infection rate. Then, a group of robotic configurations can meet two or more operations, which greatly reduces the adjustment time of preoperative positioning and is conducive to improve surgical efficiency.

Preoperative planning for the robot-assisted minimally invasive combined surgery based on the optimization algorithm has not been reported. The most important contribution of this paper is to present a preoperative planning algorithm based on the NSGA-II for RAMICA. It is worth noting that, the preoperative planning algorithm simultaneously optimizes the entry ports and configurations of the manipulators. In addition, the optimization objective functions of the preoperative planning algorithm consist of a novel global dexterity index based on the coefficient of variation to reflect the manipulator dexterity and the coordination index to reflect hand-eye coordination and instrument coordination. The preoperative planning algorithm includes the port placement constraint and the non-collision constraint to avoid unreasonable angle between the surgical instruments and the intervention of the manipulators.

This paper is organized as follows. The methods section contains the mechanical structure, mathematical models of the robot, mathematical models of the abdominal wall and surgical areas, constraints, and optimization objective functions. The results section carries out the comparative simulations and contrast experiments to illustrate the effectiveness of the preoperative planning scheme obtained by the optimization algorithm. In the conclusion section, the article is summarized and the direction of future study is also discussed.

II. METHODS

A. MECHANICAL STRUCTURE AND MATHEMATICAL MODELS OF THE ROBOT

The robot used in this study is a custom-designed robot, as shown in Figure 1. In Figure 1, the customized minimally invasive surgical robot includes a master console, a set of vision system, and a slave robot. The master console provides the interactive interface, two master manipulators and several foot switches. The master manipulator has seven degrees of freedom (DOFs). One of the seven DOFs is used to complete the clamping operation. The three joint axes converge to one point to achieve arbitrary attitude adjustment. The remaining three joints are used for any position adjustment. The foot switches are used for system control. The vision system is used to transmit the vision from the endoscope to the display equipment, which provides the surgeon with the vision information. The slave robot consists of a foundation support and three slave manipulators. Three manipulators have a similar design of passive joints and active joints. Each slave manipulator has seven DOFs. The configuration of the slave manipulator is shown in Figure 2. Passive joints include prismatic joint 1, revolute joint 2, revolute joint 3, and revolute joint 4. Active joints consist of revolute joint 5, parallelogram structure, and prismatic joint 7. The remote center motion (RCM) point is the pivot point of the surgical instrument at the entry port. Since the RCM point is a fixed point in the active joints and is not associated with changes in joint 5, joint 6, and joint 7. Therefore, the position of the RCM point is only determined by the passive joints. The revolute joint 5 and the parallelogram structure allow the surgical instrument or laparoscope to revolute around the RCM point, and the prismatic joint 7 adjusts the length of the instrument or laparoscope into the body. The slave manipulator in the middle holds the laparoscope to provide a view of the surgical area, and the other two hold the instruments to complete some surgical actions such as clamping, cutting, etc. The axis of the joint 5 is at a 45-degree angle to the horizontal line, as shown in Figure 2. The biggest difference between the laparoscope-holding manipulator and the instrument-holding manipulators is the length of the connecting rod of the passive joints, as shown in Figure 3. Owing to the passive joints
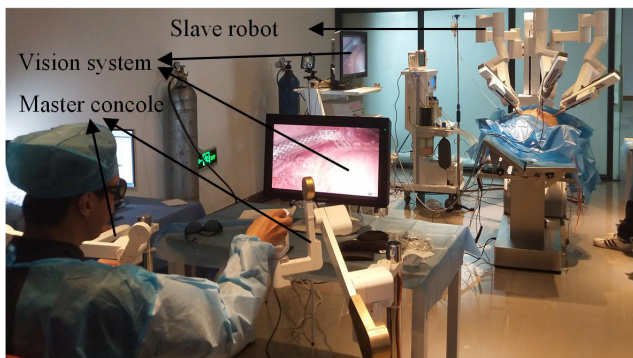

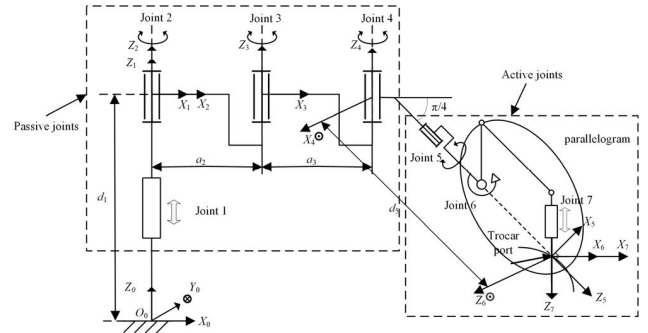**FIGURE 1.** A customized minimally invasive surgical robot.

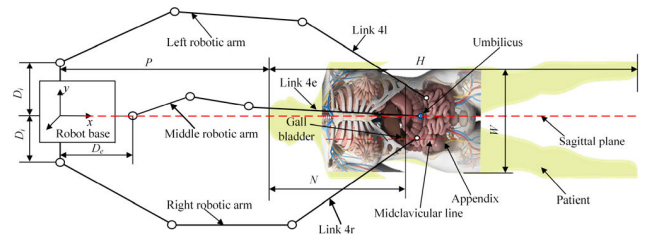**FIGURE 2.** Schematic of the robotic manipulator structure.

FIGURE 3. Sketch of the robot preoperative setting.

determine the position of the RCM point, the active joints can be simplified to a rod from joint 4 to the RCM point, and the simplified rod is called as link 4.

The modified Denavit-Hartenberg (D-H) method is adopted to build a kinematic model of the slave manipulator as shown in Figure 2. The modified D-H parameters of the slave manipulator are listed in Table 1. The global reference coordinate system $o\text{-}xyz$ is mounted on the robot base. The $o\text{-}xy$ plane coincides with the patient coronal plane, and the z-axis is perpendicular to the coronal plane pointing outward as shown in Figure 3. The distances between the axis of each revolute joint 2 of the passive joints and the z-axis of the base coordinate system are D_i and D_e, respectively. While the active joints adjust the position and posture of the end of the surgical instrument during the operations, the passive joints remain stationary. The Jacobian matrix is only related to the active joints variables and is expressed by (1), as shown at at the bottom of the next page. where $s\theta_5 = \sin\theta_5$, $c\theta_5 = \cos\theta_5$, $s\theta_6 = \sin\theta_6$, $c\theta_6 = \cos\theta_6$, and d_7 denotes the motion of prismatic joint 7. The Jacobian matrix is used for later the dexterity calculations.

TABLE 1. The modified D-H parameters of the slave manipulator.

i	α_{i-1} (rad)	a_{i-1} (mm)	d_i (mm)	θ_i (rad)
1	0	0	d_1	0
2	0	0	0	θ_2
3	0	a_2	0	θ_3
4	0	a_3	0	θ_4
5	$-3\pi/4$	0	d_5	θ_5
6	$-\pi/2$	0	0	θ_6
7	$\pi/2$	0	d_7	0

B. MATHEMATICAL MODELS OF THE ABDOMINAL WALL AND SURGICAL AREAS

In RAMICA, carbon dioxide gas is injected into the abdominal cavity to inflate the abdominal wall into an artificial pneumoperitoneum. The entry ports are located on the artificial pneumoperitoneum, and the surgical instruments need to complete the operations in the surgical areas through the entry ports. Therefore, the mathematical models of the abdominal wall and surgical areas should be developed according to the human physiological structure characteristics. The fact that the physiological structural characteristic parameters vary from person to person is taken into account, and the patient sizes are regarded as input parameters to build the mathematical model.

As an important reference point of the human physiological structure, the umbilicus has relative position relationship with many organs. The umbilicus is in the golden-ratio point of the human body height in the sagittal plane. The distance from the patient head to the base coordinate system of the robot can be measured and is denoted as P. The patient's height and width are denoted as H and W, respectively. The distance from the umbilicus to the soles of the feet is 0.618 in proportion to body height, so the ratio of the distance from the umbilicus to the top of the head to the body height, or coefficient of H, is 0.382. Thus, the position of the umbilicus based on the global reference coordinate system is expressed by (2).

$$U = (P + 0.382H, 0, c) \qquad (2)$$

The shape of the pneumoperitoneum is regarded as an ellipsoid [17]. The size of pneumoperitoneum is related to the human physiology structure and the amount of the injected gas. The lengths of the two chords in the coronal plane depend on the distance between the phalangeal union and the xiphoid process of the sternum and the distance between the sides of the umbilicus. The half of distance between the phalangeal union and the xiphoid process of the sternum is denoted as a. The half of distance between the sides of the umbilicus is denoted as b. The distance between the umbilicus and the coronal plane is denoted as c. Consequently, the mathematical model of the abdominal wall is expressed by (3).

$$\frac{(x - U_x)^2}{a^2} + \frac{y^2}{b^2} + \frac{z^2}{c^2} = 1 \qquad (3)$$

where U_x represent the x coordinate value of the umbilicus.

In RAMICA, the surgical areas are the gall bladder and the appendix. The gall bladder is located below the right lobe of the liver. More accurately, the gall bladder is approximately located in the intersection of the midclavicular line and the 12th rib. The distance between the midclavicular line and the sagittal plane is considered a quarter of body width W. The distance between the patient head and the 12th rib is easily measured as N, shown in Figure 3. In accordance with the characteristics of the human physiological structure, the surgical area of the gall bladder is approximately considered as an ellipsoid with three-chord lengths of 50mm, 100mm and 50mm, respectively. Hence, the position and shape of the gallbladder in the human body are shown in Figure 4. The mathematical model of the gall bladder is expressed by (II-B).

$$T = \left(P + N, -\frac{W}{4}, 80\right)$$

$$\left(\frac{x - T_x}{25}\right)^2 + \left(\frac{y - T_y}{50}\right)^2 + \left(\frac{z - T_z}{25}\right)^2 = 1 \qquad (4)$$

For the appendix, Mc Burney point lies between the cecum and ileum in the right lower abdomen. More accurately, Mc Burney point is two-thirds of the distance from the umbilicus to the right anterior superior iliac spine in the coronal plane. The distance between the umbilicus and the iliac joint is denoted as S and the other distance between the two iliac bones that is denoted as Q. Owing to the size of the appendix varies from person to person, the approximate shape of the appendix is considered as a cylinder with a diameter of 100mm and a height of 25mm. Therefore, the position and shape of the appendix in the human body are shown in Figure 4. The mathematical model of the appendix is expressed by (II-B).

$$AP = \left(Tx + \frac{2S}{3}, -\frac{Q}{3}, 0\right)$$

$$\left(\frac{x - AP_x}{50}\right)^2 + \left(\frac{y - AP_y}{50}\right)^2 = 1 \quad (z \in [0, 25]) \qquad (5)$$

$$J = \begin{bmatrix} -d_7 s\theta_5 s\theta_6 & d_7 c\theta_5 c\theta_6 & c\theta_5 c\theta_6 \\ \frac{\sqrt{2}}{2} d_7 c\theta_5 s\theta_6 & \frac{\sqrt{2}}{2} d_7 \left(s\theta_6 - s\theta_5 c_{\theta_6}\right) & -\frac{\sqrt{2}}{2} \left(s\theta_5 s\theta_6 + c\theta_6\right) \\ \frac{\sqrt{2}}{2} d_7 c\theta_5 s\theta_6 & \frac{\sqrt{2}}{2} d_7 \left(s\theta_6 + s\theta_5 c_{\theta_6}\right) & \frac{\sqrt{2}}{2} \left(s\theta_5 s\theta_6 - c\theta_6\right) \\ 0 & -s\theta_5 & 0 \\ -\frac{\sqrt{2}}{2} & -\frac{\sqrt{2}}{2} c\theta_5 & 0 \\ -\frac{\sqrt{2}}{2} & \frac{\sqrt{2}}{2} c\theta_5 & 1 \end{bmatrix} \qquad (1)$$
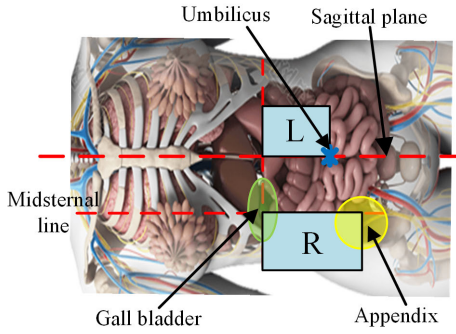
FIGURE 4. Port areas of the left and right robotic arms.

C. CONSTRAINTS AND OPTIMIZATION OBJECTIVES

The preoperative planning algorithm regards the angles of the passive joints as the design variables, and considers ranges of the port placements and the non-collision between the robot and the patient as the constraints to avoid unreasonable angle between the surgical instruments and the intervention of the manipulators. The paper proposes a novel global dexterity index and the coordination index as two optimization objective functions in the preoperative planning algorithm.

1) DESIGN VARIABLES

The joint angles of the passive joints determine port placements and the collision probability between the three slave manipulators. The link lengths of the slave manipulators of the robot-assisted minimally invasive system are immutable; therefore, the joint angles of the passive joints of the two instrument-holding manipulators are regarded as the design variables in the preoperative planning algorithm. The range of design variables are restricted as expressed in Table 2.

TABLE 2. The range of design variables.

Joint angle	θ_{l2} (rad)	θ_{l3} (rad)	θ_{l4} (rad)	θ_{r2} (rad)	θ_{r3} (rad)	θ_{r4} (rad)
Lower limit	0	$-\pi/2$	$-\pi$	$-\pi/2$	0	$-\pi/2$
Upper limit	$\pi/2$	0	$-\pi/2$	0	$\pi/2$	0

where subscript l and r represent the left slave manipulator and right slave manipulator. The subscript k is used to distinguish the two robotic arms, denotes as l and r. The design variable $\theta_{ki}(i = 2, 3, 4)$ denotes the angle of the passive joint i of the robotic arm marked k. Owing to the link lengths of the slave manipulators are constant, the position of the RCM point is determined by the angles of the passive joints. The locations of joint 4 and the RCM point are expressed by (6) and (7), respectively:

$$P_{4kx} = \begin{bmatrix} cos\,(\theta_{k2}) & cos\,(\theta_{k2} + \theta_{k3}) \end{bmatrix} \begin{bmatrix} a_{k2} \\ a_{k3} \end{bmatrix}$$

$$P_{4ky} = \begin{bmatrix} sin\,(\theta_{k2}) & sin\,(\theta_{k2} + \theta_{k3}) \end{bmatrix} \begin{bmatrix} a_{k2} \\ a_{k3} \end{bmatrix} \quad (6)$$

$$P_{5kx} = P_{4kx} - L_4 sin\,(\theta_{k2} + \theta_{k3} + \theta_{k4})$$

$$P_{5ky} = P_{4ky} + L_4 cos\,(\theta_{k2} + \theta_{k3} + \theta_{k4}) \quad (7)$$

where a_{ki} ($i = 2, 3$) denotes the length of the connecting rod between joints i and $i + 1$. L_4 denotes the length of the connecting rod between joint 4 and the RCM point in the coronal plane. P_{4kx}, P_{4ky}, P_{5kx} and P_{5ky} are the positions of the joint 4 and the RCM point in the coronal plane.

2) PORT PLACEMENT CONSTRAINT

In laparoscopic surgery, port areas are selected to be on the belly surface. Since the z-axis coordinate of any point on the belly surface is related to the x-axis coordinate and y-axis coordinate, the projection of the belly in the coronal plane should be paid more attention to. In a brief description, the port area of the left arm is located on the left side of the gall bladder and umbilicus. The port area of the middle arm is generally located on the umbilicus. The port area of the right arm is between the gall bladder and appendix in the right lower abdomen, which is convenient to take out the removed gall bladder and appendix through special tools. According to the human physiological structural parameters, the port areas of the left arm and the right arm are represented in the coronal plane by the blue-shaded rectangle marked L and R, as shown in Figure 4. The shaded area is within the motion range of the remote center point, which ensures the accessibility of the ports' areas. The ports areas of the left arm and right arm are listed in Table 3. The z-axis coordinate of each entry point can be obtained according to equation (3).

TABLE 3. The range of the ports' areas of the left arm and right arm.

Position coordinates	x_l	y_l	x_r	y_r
Lower limit	T_x	0	T_x	$-W/2$
Upper limit	AP_x	$W/3$	AP_x	$-W/4$

3) NON-COLLISION CONSTRAINT

In RAMICA, the end of the instruments can reach any position in the surgical areas, and the manipulators outside the abdominal cannot collide with each other. The entry ports and configurations of manipulators are simultaneously optimized under meeting the non-collision constraints.

The positions of the entry ports straightway affect the angles that point from the surgical instruments to the surgical areas and operational performance of the surgical instruments in the surgical areas. If the distances between the three entry ports are far between, the coordination of the surgical instruments in the surgical areas will become worse. If the distances between the three ports are too close, the robotic arms will easily collide with each other. The distances between the adjacent ports are limited to 80mm to 160mm on the projection of the coronal plane. The three entry ports should be radial from the surgical areas, and correspondingly, the robotic arms outside the abdominal are also radial rather than intersect with each other.

The joints that are most likely to collide are prismatic joint 7. The reason for the collision is the short distance between the link 4*l*, the link 4*e*, and the link 4*r*. Therefore, a safety threshold is set for the distance between the middle points of the link 4*l*, the link 4*e*, and the link 4*r*. The safety threshold is set to at least 350mm. The safety threshold is set to at least 600mm between the middle points of the link 4*l* and the link 4*r*.

If the patient has some abdominal wall wounds or other places to avoid, the port placements need to avoid these areas so as not to secondary injury or more injury that is serious.

4) A NOVEL GLOBAL DEXTERITY INDEX

The entry ports and configurations of manipulators are simultaneously optimized by preoperative planning algorithm, and that can change the kinematic performance of minimally invasive surgical robot in specific surgical areas. The reasonable kinematic performance evaluation index is necessary in the preoperative planning algorithm. The surgical instruments can flexibly reach any point in the surgical areas. In addition, two surgical instruments and the endoscope can cooperate to complete the operations such as clamping, cutting, etc.

Yoshikawa presented the concept of the manipulability ellipsoid firstly [18]. The manipulability ellipsoid described vividly the velocity and force transmission characteristics of the manipulator from joint space to task space. Yoshikawa use the volume of the manipulability ellipsoid as a measure to evaluate the isotropy of the manipulator. However, there are so many ellipsoids that have the same volume with different principal axes. Hence, the volume of the manipulability ellipsoid cannot describe reasonably the isotropy. Gosselin [19] proposed firstly the condition number that represents the ratio of the velocity and force transmission characteristics. However, the capability of the velocity and force transmission characteristics is not stated in all directions, only the ratio of maximum to minimum. Thus, the condition number does not fully describe kinematic performance. Gosselin and Angeles proposed a global condition index number [20]. The singular configuration of the manipulator is judged if the value of the global condition index is zero. Stocco *et al.* [21] presented a global isotropy index as an objective function to quantify the configuration independent isotropy of the robot. Zhang *et al.* [22] proposed a GPR-based optimization strategy to optimize port placements and robot positioning. In addition, the paper used global isotropy index and cooperation capability index as two objective functions to reflect the dexterity of the robot arm and the cooperation performance of the multi-arm, respectively. Du *et al.* [23] proposed an isotropy evaluation index based on the coefficient of variation that represents the ratio of the standard deviation σ to the mean μ. It combines all the singular values and indicates the mean and the volatility of all the data. Nevertheless, there are different data sets with the same the mean and the standard deviation. It cannot distinguish the performance between these data sets.

A novel global dexterity index *GDI* based on the coefficient of variation is proposed in this paper to comprehensively reflect the isotropy and dexterity of the manipulator. In order to distinguish the singular state of the manipulator and reflect the kinematic performance of the manipulator in the whole surgical areas, *GDI* is expressed by (8):

$$tcv = \begin{cases} \dfrac{\mu + \sigma_{min}}{\sigma}, & \sigma_{min} \neq 0 \\ 0, & \sigma_{min} = 0 \end{cases}$$

$$GDI = -\dfrac{\int\limits_w tcv \cdot dw}{\int\limits_w dw} \tag{8}$$

where σ_{min} denotes the minimum singular value of the Jacobian, σ and μ denotes the standard deviation and mean of the singular values of the Jacobian, *tcv* is a dimensionless transition index based on the coefficient of variation and comprehensively represents the isotropy and dexterity, and *w* denotes the surgical areas of the gall bladder and the appendix. It is worth to mentioning that the Jacobian matrix is normalized [24]. With the decrease of the standard deviation σ, the singular values are closer and the isotropy is better. With the increase of the mean μ or σ_{min} of the Jacobian matrix, the velocity and force transmission characteristics is better and the dexterity is higher. In a word, the isotropy and the dexterity of manipulator are preferable with the smaller the value of *GDI*.

5) THE COORDINATION INDEX

If the angle between the instruments involved in the human body is in an inappropriate state, it will be difficult to cooperate in the surgical areas even with high flexibility and isotropy, thus affecting the quality of the operation. To distinctly illustrate the angle relationship between the instruments and the endoscope, the relevant operation parameters are defined, as shown in Figure 5. The two instruments form
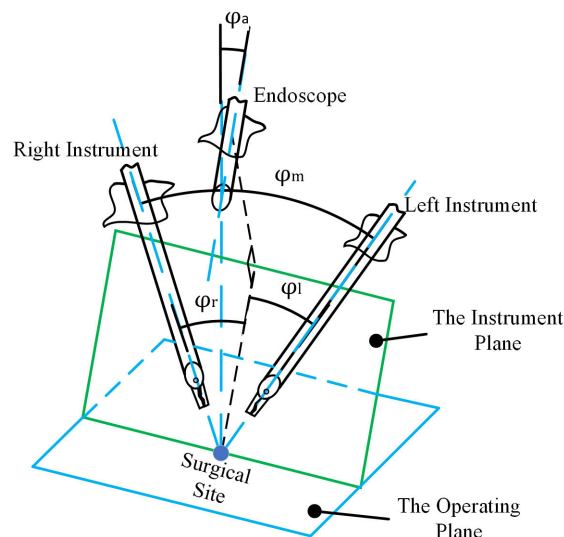
FIGURE 5. Schematic diagram of the operation parameters of the instruments and endoscope.

the instrument plane when they point to the same center point of the surgical area. The angle between two instruments is defined as the instrument angle φ_m. The angles between the projection of the endoscope on the instrument plane and the left- and right-instruments are defined as φ_l and φ_r, respectively. It is concluded that the ideal manipulation angle $\Psi_m(\Psi_m = 60°)$ by a large number of experimental statistics [25]. When φ_l is equal to φ_r, the instruments are in optimal hand-eye coordination. φ_a is the fixed azimuthal angle of the endoscope.

Owing to hand-eye coordination and instrument coordination interact with each other in the optimization process, the novel coordination index CI that reflects hand-eye coordination and instrument coordination is expressed by (9):

$$h - e = \frac{1}{2} \sum_{j=1}^{2} |\varphi_r - \varphi_l|_j$$

$$ic = \frac{1}{2} \sum_{j=1}^{2} |\varphi_m - \psi_m|_j$$

$$CI = \lambda_1 \cdot h - e + \lambda_2 \cdot ic \qquad (9)$$

where h-e and ic denote the hand-eye coordination index and instrument coordination index, respectively. λ_1 and λ_2 denote the coefficients of hand-eye coordination and instrument coordination, respectively. Where $j = 1$ and $j = 2$ denote the center point of the gall bladder and the appendix, respectively. Here, λ_1 and λ_2 are 0.5 and 0.5.

D. THE PREOPERATIVE OPTIMIZATION PROCESS

Flow chart of preoperative planning optimization algorithm based on the NSGA-II [26] consists of preparatory work, optimization process, and result processing, as shown in Figure 6. Preparatory work provides mathematical models of human physiological characteristics and robot kinematics models based on the relative position of the robot coordinate system. It also defines the generation number and population size of the optimization algorithm. In the optimization process, variable groups are first generated. If the first input data are selected as special angles such as those close to the recommended angles of surgeons, it is possible that results are the local optimal objective functions values rather than the global optimal values. Thus, the variable groups of the first generation are randomly generated in the variable ranges, while variable groups of the remaining generations are generated based on the previous variable groups that satisfy the constraints. If the variable group meets the constraints of port placements and non-interference, the optimal objective values are calculated in the surgical areas. Otherwise, the variable group is weeded out. After completing the optimization process, the optimal result graph and result table are created. Finally, the optimal preoperative planning scheme is selected according to the preoperative planning performance indexes and the actual requirements.
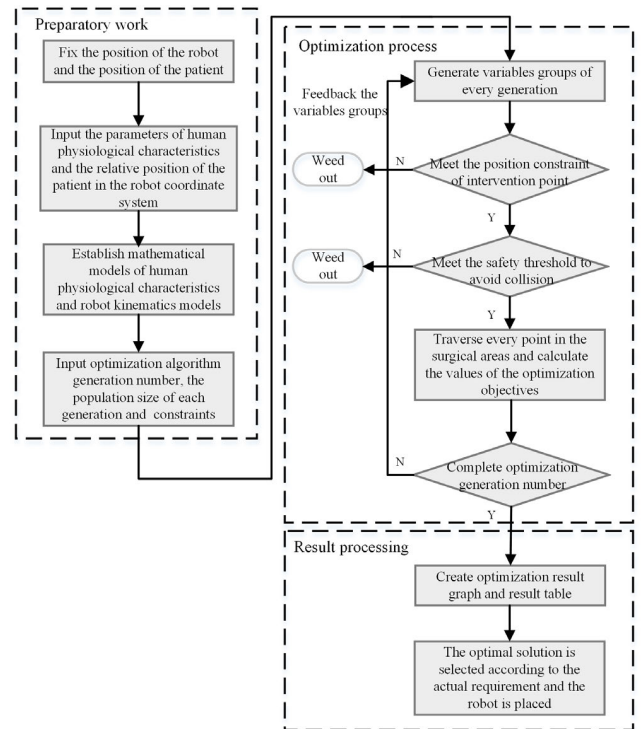

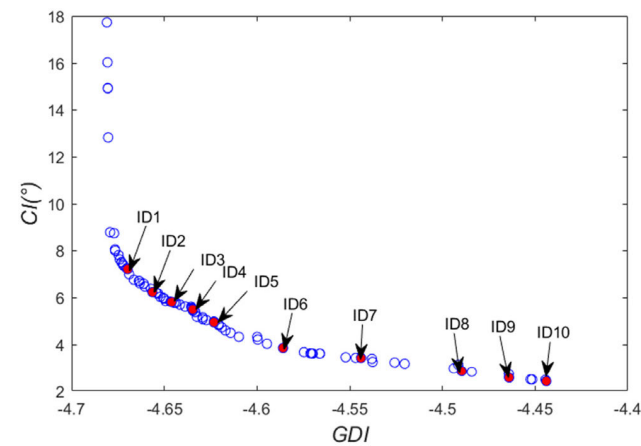FIGURE 6. Flow chart of optimization algorithm.

III. RESULTS

To validate the availability of the proposed optimization algorithm, comparative simulations and contrast experiments are designed in the paper. Three preoperative planning schemes are compared with the same surgery areas and position of the robot base, and the same serial number of the scheme represents the same scheme type in the comparative simulations and contrast experiments. Scheme I represents the preoperative planning scheme that is based on the surgeon's experiences. Scheme II has the same entry ports with the scheme I, however, the robot configurations of the scheme II is based on the optimization algorithm. Scheme III is the optimal preoperative planning scheme that is completely obtained by the proposed optimization algorithm.

According to the human physiological structure characteristics, the mathematical models of the abdominal wall, surgical areas, and port placements have been developed. This paper takes a typical human body size as an example to verify the effectiveness of the optimization algorithm. The structural size data of human body are as follows: body height H and width W are 1700mm and 360mm, respectively; the distance N that is from the patient's head to the 12th rib is approximately 540mm; the distance P that is from the patient's head to the base of the robot is 558mm. The distances D_i and D_e are 188mm and 358mm, respectively. After injecting carbon dioxide gas, the parameters a, b, and c of the belly model are 165mm, 150mm, and 200mm, respectively. The distance between the two sides of the ilium Q is 320mm. Umbilicus to ilium united S is 60mm. The MATLAB software

is used to complete the preoperative optimization process, process data, and plot figures.
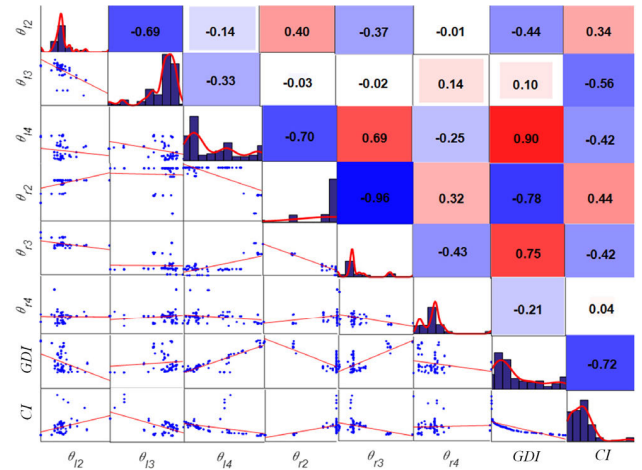
A. VERIFICATION OF THE COMPARATIVE SIMULATIONS

For RAMICA, the Pareto solution sets are as shown in Figure 7. In general, the smaller the value of the optimization objective functions, the better the dexterity and coordination of the manipulators. Due to the Pareto solution is non-inferior solution, two optimization objective functions conflict with each other. When the value of *GDI* gets smaller, the lager the value of *CI*. The scatter matrix [27] is used to represent the variation trend and dependency among the optimization objective functions and design variables. As shown in Figure 8, the correlation coefficient and scatter plot between the objective functions and design variables are distributed in the upper triangle and lower triangle of the matrix respectively, and the probability density plot of the objective functions and design variables is distributed on the diagonal of the matrix. The variation range of correlation coefficient is from −1 to 1. When the correlation coefficient is close to −1 or 1, it indicates that there is a strong correlation between the two parameters; when the correlation coefficient is close to 0, it indicates that the correlation between the two parameters is poor. In the scatter plot of the lower triangle, there is a good linear correlation between the objective functions and design variables. The following points can be known from Figure 8:
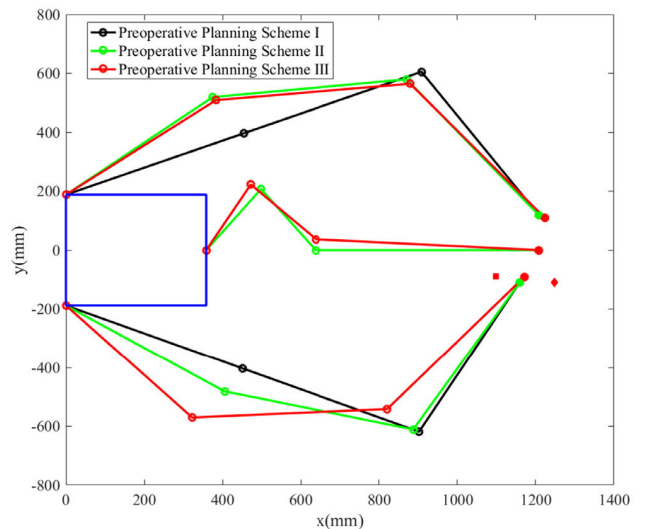

FIGURE 8. The scatter matrix of the objective functions and design variables.

so *GDI* is strongly correlated with θ_{l4}, θ_{r2}, and θ_{r3}. θ_{r2} and *GDI* has opposite trend of change.

4) The correlation coefficient between *GDI* and *CI* is -0.72, so there is a strong negative correlation between *GDI* and *CI*. When *GDI* goes up, *CI* goes down.

The optimal design variables and the optimization objective functions of ten Pareto-optimal solutions randomly chosen are listed in Table 4. The values of *GDI* are close, while the values of *CI* vary from 2.423° to 7.199°. After comprehensive consideration, the eighth preoperative planning scheme in Table 4 is selected as the final preoperative planning scheme. The configurations of the manipulators and locations of entry ports of the three preoperative planning schemes on the *o-xy* plane are shown in Figure 9. Scheme I and scheme II have the same entry ports, and their entry ports are close to entry ports of scheme III. The black lines represent the linkages of the preoperative planning scheme I, and the black solid circles represent the entry ports. The

FIGURE 7. Pareto-optimal solution sets of the two optimization objectives.

1) The correlation coefficient between θ_{l2} and θ_{l3} is -0.69, so there is a strong negative correlation between θ_{l2} and θ_{l3}. When θ_{l2} increases, θ_{l3} decreases.

2) The correlation coefficients between θ_{l4} and θ_{r2}, θ_{l4} and θ_{r3}, θ_{r2} and θ_{r3} are -0.7, 0.69 and -0.96 respectively, so θ_{l4}, θ_{r2}, and θ_{r3} are strongly correlated. When θ_{r2} gets smaller, the bigger θ_{l4} and θ_{r3} get.

3) The correlation coefficients between *GDI* and θ_{l4}, *GDI* and θ_{r2}, *GDI* and θ_{r3} are 0.9, -0.78, 0.75 respectively,

FIGURE 9. Configurations of three preoperative planning schemes.

TABLE 4. Ten Pareto-optimal solutions.

ID	Design variable						Objective functions	
	θ_{l2}(rad)	θ_{l3}(rad)	θ_{l4}(rad)	θ_{r2}(rad)	θ_{r3}(rad)	θ_{r4}(rad)	GDI	CI (°)
1	0.6984	-0.5625	-2.7658	-0.8669	0.9235	-0.7179	-4.669	7.199
2	0.6956	-0.5532	-2.7547	-0.8658	0.9222	-0.7163	-4.656	6.224
3	0.6959	-0.5521	-2.7471	-0.8673	0.9241	-0.7163	-4.646	5.806
4	0.6973	-0.5468	-2.7479	-0.8673	0.9221	-0.7162	-4.635	5.489
5	0.6924	-0.5393	-2.7429	-0.8658	0.9224	-0.7182	-4.623	4.947
6	0.7004	-0.5661	-2.6914	-0.8658	0.9224	-0.7167	-4.586	3.854
7	0.6955	-0.5641	-2.6647	-0.8658	0.9224	-0.7169	-4.544	3.427
8	0.6977	-0.5863	-2.6069	-0.8706	0.9284	-0.7183	-4.489	2.859
9	0.6868	-0.5681	-2.6067	-0.8706	0.9281	-0.7167	-4.464	2.574
10	0.6766	-0.5495	-2.6113	-0.8737	0.932	-0.7179	-4.444	2.423

TABLE 5. The optimization objective function values of the three preoperative planning schemes in the comparative simulations.

	GDI (*left*)	GDI (*right*)	*ic* (°)	*h-e* (°)	GDI	CI (°)
Scheme I	-3.9949	-4.3211	8.197	10.481	-4.158	9.339
Scheme II	-4.2929	-4.3591	8.197	10.481	-4.326	9.339
Scheme III	-4.5165	-4.4624	2.846	2.871	-4.489	2.859

green lines represent the linkages of the preoperative planning scheme II, and the green solid circles represent the entry ports. The green and black lines of the middle arm are coincident. The red lines represent the linkages of the preoperative planning scheme III, and the red solid circles represent the entry ports. The blue square represents the robot base, the red square represents center point of the gall bladder and the red diamond represents center point of the appendix.

In the same simulation environment, the objective function values of the three preoperative planning schemes are listed in Table 5. For the sake of making a detailed comparison between the three preoperative planning schemes, left arm dexterity, right arm dexterity, *ic*, and *h-e* in the surgical areas are all compared as reference indexes in addition to the two optimization objective functions. When the value of *GDI* is smaller, the better the dexterity of the manipulator. It means that the manipulator can freely reach the arbitrary point in the surgical areas. When the value of *ic* is increased, the angle between the instruments is further from the ideal coordination angle, which means it's harder for two instruments to work together. It is similar that the value of *h-e* is risen, the hand-eye coordination is worse. The value of *GDI* of the scheme III is about 7.96% and 3.77% less than scheme I and scheme II. Nevertheless, the value of *ic* and the value of *h-e* of the scheme III are about 65.28% and 72.61% less than scheme I and scheme II, respectively. The value of *CI* of the scheme III is about 69.39% less than scheme I and scheme II. It represents that the hand-eye coordination and instrument coordination of the scheme III are much better than the others. And the hand-eye coordination changes more than the instrument coordination in the scheme III. Scheme I and scheme II have the same values of *CI* because they have the same entry ports. In sum, it is obvious that scheme II is

slightly better than scheme I, and scheme III is better than scheme II and scheme I. The effectiveness of the preoperative planning scheme based on the optimization algorithm is verified by the comparative simulations.

The comparison between results of reference [12], [17], and optimization algorithm is listed in Table 6. References [12] and [17] used cholecystectomy as an example for preoperative planning optimization. Reference [12] optimized the configurations of the manipulators based on the given entry ports by the improved gradient projection method and maximum distance criterion. However, the previous study did not optimize the entry ports. In fact, the hand-eye coordination index and instrument coordination index depend on the locations of the entry ports. Table 6 shows a comparison of the previous study results (ID 1) with the preoperative optimization results in this paper (ID 3). The global dexterity index and the coordination index of ID3 were about 9.86% and 69.48% than ID1. The optimization process in reference [17] was divided entry ports optimization and manipulator configuration optimization into two processes. The interaction between dexterity and coordination was not considered. The global dexterity index and the coordination index of ID3 were about 15% and 57.41% than ID2.

B. VERIFICATION OF THE CONTRAST EXPERIMENTS

In addition to the comparative simulations, the contrast experiments of three preoperative planning schemes are also conducted to confirm the effectiveness of the preoperative planning scheme based on the preoperative optimization algorithm. The three preoperative planning schemes in the contrast experiments are based on the actual human body model and the viscera models. For RAMICA, the manipulator configurations and the initial instrument poses of three

TABLE 6. Comparison between results of reference [12], [17], and optimization algorithm.

ID	GDI (left)	GDI (right)	ic (°)	h-e (°)	GDI	CI (°)
1	-4.113	-4.059	12.408	6.326	-4.086	9.367
2	-3.974	-3.838	9.372	4.052	-3.906	6.712
3	-4.5165	-4.4624	2.846	2.871	-4.489	2.859

TABLE 7. The optimization objective function values of the three preoperative planning schemes in the contrast experiments.

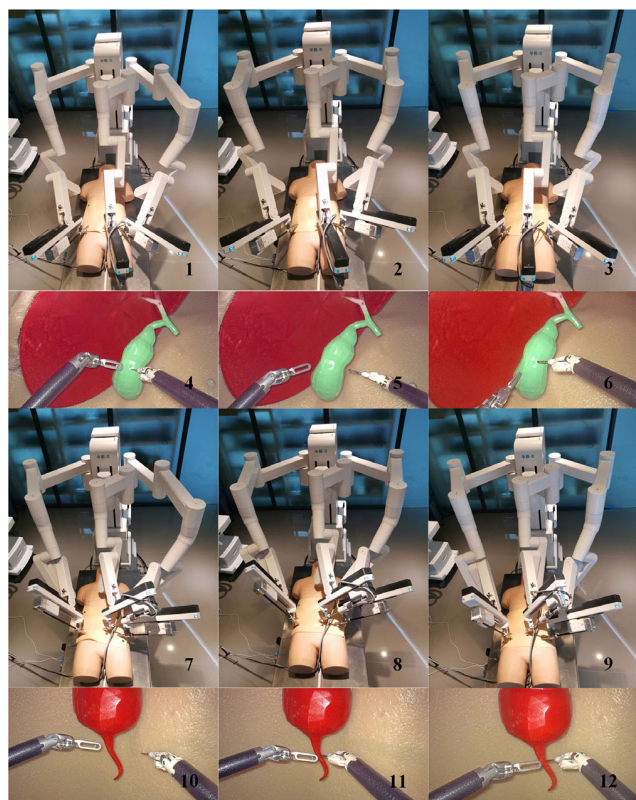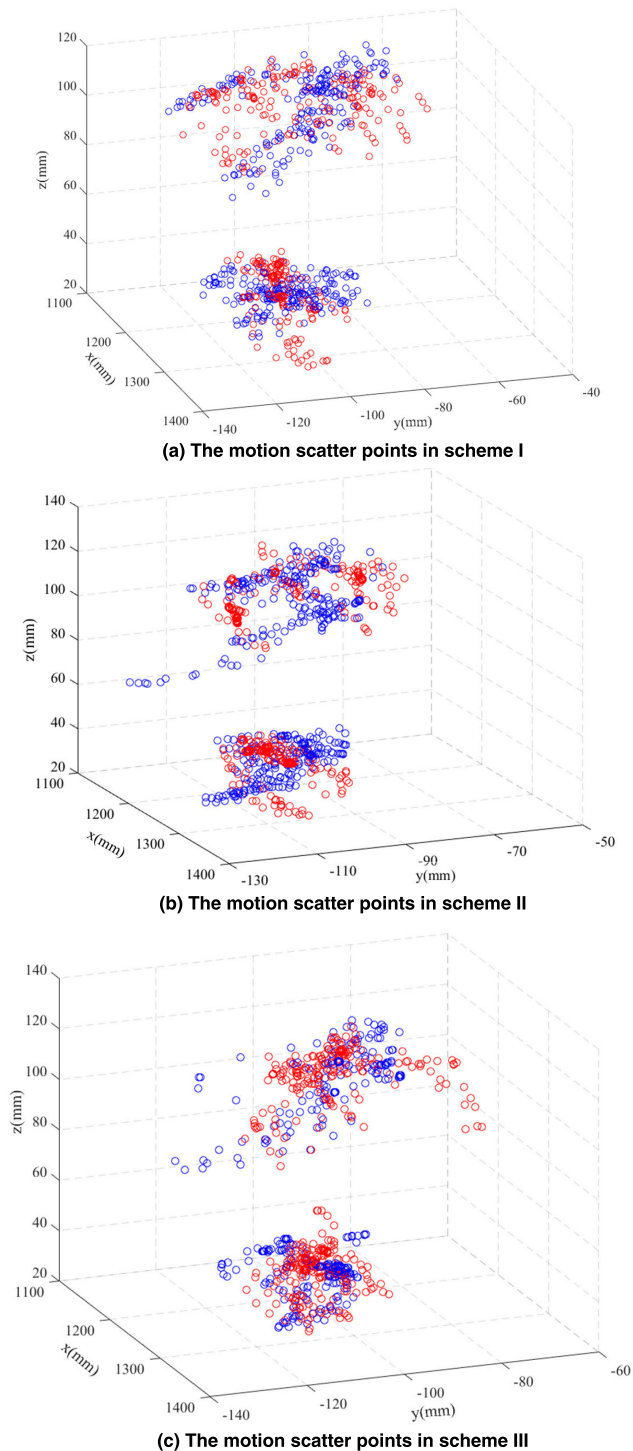|	GDI (left)	GDI (right)	ic (°)	h-e (°)	GDI	CI (°)
Scheme I	-4.083	-4.182	5.58	11.89	-4.133	8.74
Scheme II	-4.349	-4.228	5.58	11.89	-4.289	8.74
Scheme III	-4.375	-4.373	2.75	3.01	-4.374	2.88

FIGURE 10. The configurations of manipulators and the initial poses of the instruments of three preoperative planning schemes.

The three preoperative planning schemes in the contrast experiments are based on the mathematic model and the whole surgical areas. There is different from the comparative simulations that the contrast experiments perform surgical operations on the viscera models and partly traverse the surgical areas, while the comparative simulations integrally traverse the whole two surgical areas. In the contrast experiments, a series of scattered points are uniformly selected within the motion time range to represent the motion range of the surgical instruments. The movement points of the surgical instruments for the three preoperative planning schemes are shown in Figure 11. The three figures from (a) to (c) in Figure 11 correspond to schemes I to III in turn. Each subgraph shows the movement range of the left and right instruments in the two surgical areas under the corresponding scheme. The red circles represent the motion scatter of the right instrument, while the blue circles represent the motion scatter of the left instrument. The scattered points of the instruments in the surgical areas cover the peripheries of the surgical areas. The scattered points in Figure 11 are used to calculate robot kinematic performances, and the evaluation index values are shown in Table 7. The value of *GDI* of the scheme III is about 5.83% and 1.98% less than scheme I and scheme II. The value of *ic* and the value of *h-e* of the scheme III are about 50.72% and 74.68% less than scheme I and scheme II, respectively. The value of *CI* of the scheme III is about 67.05% less than scheme I and scheme II. It represents that the hand-eye coordination and instrument coordination of the scheme III are much better than the others. And the instrument coordination changes more than the hand-eye coordination in the scheme III. The *GDI* values of the three schemes are close to each other, the all evaluation index values of scheme III are almost better than that of scheme I and scheme II. It demonstrates the effectiveness of the preoperative planning scheme based on the optimization algorithm by the contrast experiments.

Because the ergodic points of the surgical instruments are different in the comparative simulations and contrast experiments, the optimization objective function values are different. The optimization objective function values of scheme III are superior to other two schemes.

preoperative planning schemes are shown in Figure 10. Figure 10 is divided into three columns and four rows. The left-most column, the middle column, and the right-most column corresponds to the entry ports and manipulator configurations of scheme I, scheme II, and scheme III respectively. The first and third rows represent the manipulator configurations with the instruments pointing to the gallbladder and appendix, respectively. The second and fourth rows represent the initial poses of the instruments in the endoscopic view when the instruments point to the gallbladder and appendix, respectively.

(a) The motion scatter points in scheme I

(b) The motion scatter points in scheme II

(c) The motion scatter points in scheme III

FIGURE 11. A series of motion scatter points of three preoperative planning schemes.

IV. CONCLUSION

In this paper, a preoperative planning algorithm based on the NSGA-II is proposed to improve the dexterity and coordination of the manipulators in the surgical areas and to reduce the preoperative adjustment time for RAMICA. The optimization objective functions of the preoperative planning algorithm consisted of a novel global dexterity index based on the coefficient of variation and the coordination index. The preoperative planning algorithm took the port placement constraint and the non-collision constraint into account. In the comparative simulations, the value of *GDI* of the scheme III is about 7.96% and 3.77% less than scheme I and scheme II, and the value of *CI* of the scheme III is about 69.39% less than scheme I and scheme II. In the contrast experiments, the value of *GDI* of the scheme III is about 5.83% and 1.98% less than scheme I and scheme II, and the value of *CI* of the scheme III is about 67.05% less than scheme I and scheme II. The comparative simulations and contrast experiments demonstrate the effectiveness and superiority of the preoperative planning scheme obtained by the optimization algorithm. The preoperative planning algorithm help the surgeon to reduce the adjusting time and improve the kinematic performances (the global dexterity, the instrument coordination, and the hand-eye coordination) for different physiological structural characteristic parameters of patients and different combined surgery. The preoperative planning algorithm can be applied to other robot-assisted minimally invasive combined surgery by modifying the physiological structural characteristic parameters, the constraints, surgical areas, and optimization objective functions. The preoperative planning algorithm can be applied to the surgical training system. In the future, the preoperative planning algorithm can be applied in clinical surgery to provide guidance for preoperative planning.

REFERENCES

[1] G. Niu, B. Pan, Y. Fu, and C. Qu, "Development of a new medical robot system for minimally invasive surgery," *IEEE Access*, vol. 8, pp. 144136–144155, Aug. 2020.

[2] R. H. Taylor and D. Stoianovici, "Medical robotics in computer-integrated surgery," *IEEE Trans. Robot. Autom.*, vol. 19, no. 5, pp. 765–781, Oct. 2003.

[3] G. S. Ferzli and A. Fingerhut, "Trocar placement for laparoscopic abdominal procedures: A simple standardized method," *J. Amer. College Surgeons*, vol. 198, no. 1, pp. 163–173, Jan. 2004.

[4] WELCH, and E. Claude, "Diagnosis of acute abdominal disease," *Ann. Surg.*, vol. 192, no. 2, pp. 266–267, Aug. 1980.

[5] D. L. Pick, D. I. Lee, D. W. Skarecky, and T. E. Ahlering, "Anatomic guide for port placement for DaVinci robotic radical prostatectomy," *J. Endourol.*, vol. 18, no. 6, pp. 572–575, Aug. 2004.

[6] K. K. Badani, F. Muhletaler, M. Fumo, S. Kaul, J. O. Peabody, M. Bhandari, and M. Menon, "Optimizing robotic renal surgery: The lateral camera port placement technique and current results," *J. Endourol.*, vol. 22, no. 3, pp. 507–510, Mar. 2008.

[7] J. W. Cannon, J. A. Stoll, S. D. Selha, P. E. Dupont, R. D. Howe, and D. F. Torchiana, "Port placement planning in robot-assisted coronary artery bypass," *IEEE Trans. Robot. Autom.*, vol. 19, no. 5, pp. 912–917, Oct. 2003.

[8] L. Adhami, E. Coste-Maniere, and J. Boissonnat, "Planning and simulation of robotically assisted minimal invasive surgery," in *Proc. MICCAI*, Pittsburgh, PA, USA, Oct. 2000, pp. 107–108.

[9] L. Adhami and E. Coste-Manière, "Optimal planning for minimally invasive surgical robots," *IEEE Trans. Rob. Autom.*, vol. 19, no. 5, pp. 854–863, Oct. 2003.

[10] A. L. Trejos and R. V. Patel, "Port placement for endoscopic cardiac surgery based on robot dexterity optimization," in *Proc. IEEE Int. Conf. Robot. Autom.*, Barcelona, Spain, Apr. 2005, pp. 912–917.

[11] H. Azimian, J. Breetzke, A. L. Trejos, R. V. Patel, M. D. Naish, T. Peters, J. Moore, C. Wedlake, and B. Kiaii, "Preoperative planning of robotics-assisted minimally invasive coronary artery bypass grafting," in *Proc. IEEE Int. Conf. Robot. Autom.*, Anchorage, AK, USA, May 2010, pp. 1548–1553.

[12] G. Li, D. Wu, R. Ma, K. Huang, and Z. Du, "Pose planning for robotically assisted minimally invasive surgery," in *Proc. 3rd Int. Conf. Biomed. Eng. Informat.*, Yantai, China, Oct. 2010, pp. 1769–1774.

[13] L. Yu, Z. Wang, L. Sun, W. Wang, and L. Wang, "Research on preoperative positioning analysis of instrument arms for minimally invasive surgical robot," in *Proc. IEEE Int. Conf. Mechatronics Autom.*, Tianjin, China, Aug. 2014, pp. 1269–1275.

[14] M. Feng, X. Jin, W. Tong, X. Guo, J. Zhao, and Y. Fu, "Pose optimization and port placement for robot-assisted minimally invasive surgery in cholecystectomy," *Int. J. Med. Robot. Comput. Assist. Surg.*, vol. 13, no. 4, p. e1810, Dec. 2017.

[15] Y. Chen, S. Wu, and J. Kong, "Transumbilical single-incision laparoscopic combined cholecystectomy and appendectomy: A retrospective comparative study," *J. Laparoendoscopic Adv. Surgical Techn.*, vol. 24, no. 10, pp. 702–706, Oct. 2014.

[16] W. Cai, J. Xu, M. Zheng, M. Qin, and H. Zhao, "Combined laparoendoscopic single-site surgery: Initial experience of a single center," *Hepatogastroenterology*, vol. 59, no. 116, pp. 986–989, Mar. 2012.

[17] J. Yang, L. T. Yu, and L. Wang, "Preoperative planning of intraperitoneal minimally invasive surgery robot based on characteristic parameters and double cooperative spaces," *Robot*, vol. 39, no. 2, pp. 230–238, Mar. 2017.

[18] T. Yoshikawa, "Manipulability of robotic mechanisms," *Int. J. Robot. Res.*, vol. 4, no. 2, pp. 3–9, Jun. 1985.

[19] C. M. Gosselin, "Dexterity indices for planar and spatial robotic manipulators," in *Proc. IEEE Int. Conf. Robot. Autom.*, Cincinnati, OH, USA, May 1990, pp. 650–655.

[20] C. Gosselin and J. Angeles, "A global performance index for the kinematic optimization of robotic manipulators," *J. Mech. Des.*, vol. 113, no. 3, pp. 220–226, Sep. 1991.

[21] L. Stocco, S. E. Salcudean, and F. Sassani, "Fast constrained global minimax optimization of robot parameters," *Robotica*, vol. 16, no. 6, pp. 595–605, Nov. 1998.

[22] F. Zhang, Z. Yan, and Z. Du, "Preoperative setup planning for robotic surgery based on a simulation platform and Gaussian process," in *Proc. IEEE Int. Conf. Mechatronics Autom.*, Harbin, China, Aug. 2016, pp. 902–907.

[23] Z. Du, W. Wang, W. Wang, and W. Dong, "Preoperative planning for a multi-arm robot-assisted minimally invasive surgery system," *Simulation*, vol. 93, no. 10, pp. 853–867, Jul. 2017.

[24] I. Fassi, G. Legnani, and D. Tosi, "Geometrical conditions for the design of partial or full isotropic hexapods," *J. Robot. Syst.*, vol. 22, no. 10, pp. 207–518, Oct. 2005.

[25] S. Selha, P. Dupont, R. D. Howe, and D. F. Torchiana, "Dexterity optimization by port placement in robot-assisted minimally invasive surgery," *Proc. SPIE*, vol. 4570, pp. 97–104, Feb. 2002.

[26] K. Deb, A. Pratap, S. Agarwal, and T. Meyarivan, "A fast and elitist multiobjective genetic algorithm: NSGA-II," *IEEE Trans. Evol. Comput.*, vol. 6, no. 2, pp. 182–197, Apr. 2002.

[27] R. Ur-Rehman, S. Caro, D. Chablat, and P. Wenger, "Multi-objective path placement optimization of parallel kinematics machines based on energy consumption, shaking forces and maximum actuator torques: Application to the orthoglide," *Mechanism Mach. Theory*, vol. 45, no. 8, pp. 1125–1141, Aug. 2010.

TAO SONG is currently pursuing the Ph.D. degree with the State Key Laboratory of Robotics and System, Department of Mechatronics Engineering, Harbin Institute of Technology, China. His research interests include medical robot, preoperative planning, and kinematic calibration.

BO PAN received the Ph.D. degree in mechatronics engineering from the Harbin Institute of Technology, China, in 2009. He is currently an Associate Professor with the State Key Laboratory of Robotics and System, Harbin Institute of Technology. His research interests include robotic optimization design, robotic control, and medical robotics.

GUOJUN NIU received the Ph.D. degree in mechatronics engineering from the Harbin Institute of Technology, China, in 2017. He is currently a Lecturer with the School of Mechanical Engineering and Automation, Zhejiang Sci-Tech University, China. His research interests include robotic optimization design, control, and medical robotics.

YILI FU (Member, IEEE) received the Ph.D. degree in mechatronic engineering from the Harbin Institute of Technology, China, in 1996. He is currently a Professor with the State Key Laboratory of Robotics and System, Harbin Institute of Technology. His research interests include space robotics, medical robotics, and mobile robotics.

● ● ●